Raman and infrared properties and layer dependence of the phonon dispersions in multilayered graphene

Jin-Wu Jiang,[1,*] Hui Tang,[2,1] Bing-Shen Wang,[3] and Zhao-Bin Su[1,4]
[1]*Institute of Theoretical Physics, Chinese Academy of Sciences, Beijing 100080, People's Republic of China*
[2]*Institute of Physics, Chinese Academy of Sciences, Beijing 100190, People's Republic of China*
[3]*State Key Laboratory of Semiconductor Superlattices and Microstructures and Institute of Semiconductors, Chinese Academy of Sciences, Beijing 100083, People's Republic of China*
[4]*Center for Advanced Study, Tsinghua University, Beijing 100084, People's Republic of China*
(Received 6 September 2007; revised manuscript received 10 April 2008; published 13 June 2008)

The symmetry group analysis is applied to classify the phonon modes of *N*-stacked graphene layers (NSGLs) with *AB* and *AA* stacking, particularly their infrared and Raman properties. The dispersions of various phonon modes are calculated in a multilayer vibrational model, which is generalized from the lattice vibrational potentials of graphene to including the interlayer interactions in NSGLs. The experimentally reported redshift phenomena in the layer-number dependence of the intralayer optical *C*-*C* stretching mode frequencies are interpreted. An interesting low-frequency interlayer optical mode is revealed to be Raman or infrared active in even or odd NSGLs, respectively. Its frequency shift is sensitive to the layer number and saturated at about 10 layers.

DOI: 10.1103/PhysRevB.77.235421 PACS number(s): 81.05.Uw, 63.22.−m

I. INTRODUCTION

In recent years, the ultrathin graphite films, i.e., N (>1) stacked graphene layers (NSGLs), is successfully fabricated.[1,2] Extensive studies have been devoted to these systems due to their competitive capability for the design of novel nanodevices. It is desirable to carry out a through symmetry analysis to figure out the corresponding electron and phonon spectra, and to reveal the relevant selection rules and the optical activities. Moreover, to our knowledge, although there are some studies on the electronic structure,[3] no existing works concern the phonon dispersions for the NSGLs. Recently it has been reported that the frequencies of the optical *C*-*C* stretching mode in the NSGLs decrease with increasing N.[4–6] The amplitude of this redshift is about 3–5, 5–6, and 8 cm^{-1} in these three experiments, respectively. Theoretical explanation of this redshift is required.

In this paper, the symmetry analysis is referred to for both the *AB*- and *AA*-stacked lattice structures, while the latter has the point group D_{6h} irrespective of the even-oddness of N. We classify the phonon normal modes at the Γ point and determine their Raman and infrared (ir) properties. We generalize the force-constant model of graphene[7] into NSGLs and it can be applied to calculate the phonon dispersions for the NSGLs in *AB* or *AA* stacking with arbitrary layer number N.

For the intralayer optical *C*-*C* stretching mode with frequency around 1600 cm^{-1}, it is Raman active for all NSGLs and the calculated frequencies exhibit layer-number dependence as the frequency decreases with increasing N. The redshift values for the *AB*- (*AA*-) stacked systems are about 2 cm^{-1} (4 cm^{-1}) which are consistent with the experimental measurements. In the medium frequency range around 800 cm^{-1}, the out-of-plane optical mode is ir active for *AB*-stacked structure but neither Raman nor ir active in *AA* stacking. Its frequency behaves as a blueshift as layer number increases. There is an interesting interlayer optical mode in the low-frequency region which is Raman active in the NSGLs with N even (ENSGLs) while ir active in NSGLs with N odd (OENSGLs). Its frequency value depends on the layer number N more sensitively and increases from 106 cm^{-1} (94.5 cm^{-1}) to 149.8 cm^{-1} (133.6 cm^{-1}) for the *AB*- (*AA*-) stacked NSGLs, which is of an order less than those intralayer optical modes. Phonon dispersions for the *AA*-stacked three-dimensional (3D) graphite are also discussed.

The present paper is organized as follows. In Sec. II, the lattice configuration is illustrated for the NSGLs. Section III is devoted to the symmetry analysis for the phonon modes. The vibrational potential energy is discussed in Sec. IV A, while the main results and relevant discussions on phonon spectrum calculations are presented in Sec. IV B. The paper ends with a brief summary in Sec. V.

II. LATTICE CONFIGURATION

A. *AB* stacked

It is known that graphene is a single layer of carbon atoms with the honeycomb lattice configuration which is characterized by the D_{6h} symmetry.[8] The 3D graphite is an *AB*-stacked honeycomb lattice, where the *B* layers are achieved by shifting the *A* layers along one of its first-nearest carbon-carbon bonds in the horizontal plane as shown in Fig. 1(a). The space group of the 3D graphite is nonsymmorphic group D_{6h}^4 with nonprimitive translation $\vec{\tau}=\frac{1}{2}\vec{c}$ (primitive translation $\vec{t}=n_1\vec{a}_1+n_2\vec{a}_2+n_3\vec{c}$).[9] The distance between two adjacent layers is about $\frac{c}{2}=3.35$ Å which is much larger than the bond length between two nearest-neighbor atoms in the plane, $b=1.42$ Å.

The NGSLs are also constructed by the *AB*-stacked honeycomb lattice, but with limited number of layers. Although the structures of each layer of 3D graphite and NSGLs are the same, the corresponding symmetry groups are different

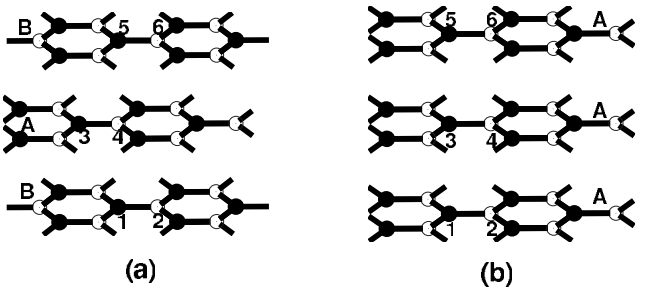

FIG. 1. The sketch of the configurations of *AB* stacked in (a) and *AA* stacked in (b) for multilayer graphene.

since the displacement symmetry along $\vec{c}$ axis no longer exists for NSGLs, so does the symmetry associated with $\vec{\tau}$. Now the symmetry group becomes a direct product of a 3D point group and a 2D translational group. Moreover, the point groups are different for ENSGLs and ONSGLs as mentioned in Ref. 10. For the ENSGLs, a center of inversion σ_i occurs in the middle of atom 4 in the $\frac{N}{2}$th layer and 5 in the $\frac{N}{2}+1$th layer as shown in Fig. 1(a). There are one threefold main axis in the direction perpendicular to the layers and three twofold axes C_2'' perpendicular to the main axis and at angles of $\pi/3$ to each other. All these symmetry operations together constitute the point group $D_{3d}=\{E,3C_3,3C_2''\}\times\{E,\sigma_i\}$. In the ONSGLs, instead of a center of inversion there is a reflection symmetry σ_h with the middle layer as its reference plane. A threefold main axis exists in the direction of the z axis and three twofold axes C_2' are perpendicular to it. We notice that these three twofold axes C_2' are one to one perpendicular to those of C_2''. Consequently, the symmetry group for the ONSGLs is $D_{3h}=\{E,3C_3,3C_2'\}\times\{E,\sigma_h\}$.

The environments for an atom in the graphite and NSGLs are different from that in 2D graphene. For each carbon atom in the graphene layer, there are three nearest-neighbor carbon atoms and six next-nearest neighbors. There are four carbon atoms, 1–4, in a unit cell of graphite, as represented in Fig. 1(a). For atom 4 in the A layer, there are two interlayer nearest neighbors in each of the two adjacent layers, with the distance c. Also, in each of the two adjacent layers, there are three interlayer next-nearest-neighbor atoms around atom 4 with distance $\sqrt{b^2+(\frac{c}{2})^2}$. As illustrated in Fig. 1(a), the adjacent environment for atom 3 is quite different from that of atom 4. It has no interlayer first neighbors with the same distance as $\frac{c}{2}$. However, atom 3 has six interlayer neighbors in each of the two adjacent layers with the same distance as that of the second-nearest neighbor of atom 4.

B. *AA* stacked

The *AA*-stacked NSGLs (*AA*-NSGLs) are constructed by an *AA*-stacked honeycomb lattice where all layers have the same configuration. In the *AA*-stacked system, the ENSGLs, ONSGLs, and the 3D graphite have the same point group D_{6h} which is the symmetry of the graphene. As shown in Fig. 1(b), the environments for carbon atoms in the *AA*-stacked NSGLs are quite different from those in the *AB*-stacked systems. For each atom, there are two interlayer nearest neighbors in each of the two adjacent layers with the distance $\frac{c}{2}$. Moreover, each atom has six interlayer second-nearest neighbors with distance $\sqrt{b^2+(\frac{c}{2})^2}$ in its two adjacent layers. We notice here that in the *AA*-stacked 3D graphite, there are only two atoms in the unit cell and the primitive translation along the c axis is $\vec{c}/2$, which is half of the correspondence in the *AB*-stacked 3D graphite.

III. SYMMETRY ANALYSIS FOR THE PHONON MODES

The dynamical representation $\Gamma^{\text{dyn}}=\Gamma^{v}\otimes\Gamma^{\text{atom}}$ can be decomposed into the irreducible representations of the symmetry group, with the lattice displacements as the bases, where Γ^{v} is the vector representation and Γ^{atom} is the permutation representation of the group. By applying the projection operator technique, we carry out the decomposition of the dynamical representation into the irreducible representations for the NSGLs with N even and odd, respectively. According to Elliott,[11] the ir active phonon modes belong to the irreducible representations decomposed from the vector representa-

TABLE I. The symmetry analysis for the phonon modes at the Γ point of the NSGLs with *AA* or *AB* stacking. Phonon modes are classified by the irreducible representations of Γ^{dyn} in the fourth column. The irreducible representations of the ir and Raman-active modes are listed in the fifth and sixth columns, respectively.

		Group	Γ^{dyn}	Γ^{Ir}	Γ^{R}
Graphene[a]		D_{6h}	$A_{2u}\oplus B_{2g}\oplus E_{1u}\otimes E_{2g}$	/	E_{2g}
AB stacked	ENSGLs	D_{3d} [b]	$N(A_{1g}\oplus A_{2u}\oplus E_g\oplus E_u)$	$(N-1)A_{2u}\oplus(N-1)E_u$	$NA_{1g}\oplus NE_g$
	ONSGLs	D_{3h} [b]	$(N-1)A_1'\oplus(N+1)A_2''\oplus(N+1)E'\oplus(N-1)E''$	$NA_2''\oplus NE'$	$(N-1)A_1'\oplus NE'\oplus(N-1)E''$
	3D[c]	D_{6h}^4	$2(A_{2u}\oplus B_{2g}\oplus E_{1u}\oplus E_{2g})$	$A_{2u}\oplus E_{1u}$	$2E_{2g}$
AA stacked	ENSGLs	D_{6h}	$\frac{N}{2}(A_{1g}\oplus A_{2u}\oplus B_{1u}\oplus B_{2g}\oplus E_{1u}\oplus E_{1g}\oplus E_{2g}\oplus E_{2u})$	$(\frac{N}{2}-1)(A_{2u}\oplus E_{1u})$	$\frac{N}{2}(A_{1g}\oplus E_{1g}\oplus E_{2g})$
	ONSGLs	D_{6h}	$\frac{N-1}{2}(A_{1g}\oplus B_{1u}\oplus E_{1g}\oplus E_{2u})\oplus\frac{N+1}{2}(A_{2u}\oplus B_{2g}\oplus E_{1u}\oplus E_{2g})$	$\frac{N-1}{2}(A_{2u}\oplus E_{1u})$	$\frac{N-1}{2}(A_{1g}\oplus E_{1g})\oplus\frac{N+1}{2}E_{2g}$
	3D	D_{6h}	$A_{2u}\oplus B_{2g}\oplus E_{1u}\oplus E_{2g}$	/	E_{2g}

[a]Reference 8.
[b]Reference 10.
[c]Reference 13.

TABLE II. Comparison of several mode frequencies (in the unit of cm^{-1}) for the *AB*-stacked 3D graphite between our calculation results and the experimental values (Refs. 19 and 20).

Reps	A_1'	E_{2g}	A_{2u}	E_{2g}
Experiments	30[a]	40[a]	868[b]	1586[b]
Theory	30.2	42.7	869.9	1586.6

[a]Reference 19.
[b]Reference 20.

tion Γ^v, while the Raman-active modes correspond to the irreducible representations shown up in the decomposition of a six-dimensional representation with bases as the quadratic forms: x^2+y^2, z^2, x^2-y^2, xy, yz, and zx. The three acoustic modes with zero frequency at the Γ point, which correspond to the vector representation Γ^v, are excluded in the consideration of ir and Raman-active modes. For comparison the corresponding results for the graphene and 3D graphite are also listed in the following. The symbol for the irreducible representations we used here is the notation used in Ref. 12 which is the most commonly used in the treatment of molecules.

The symmetry analysis for the phonon modes and the Raman and ir modes is classified in Table I. In the *AB*-stacked NSGLs, since the σ_i symmetry and σ_h symmetry cannot coexist in the ENSGLs or ONSGLs, we can see two straightforward consequences from the above classification for the ir and Raman-active modes. First, in the ENSGLs, phonon modes cannot be ir and Raman active simultaneously (which is also true for the graphene and graphite). However, in the ONSGLs, the N E' modes are both ir and Raman active. This is because there is no inversion center in the ONSGLs. Second, among the optical modes with their vibrational displacements perpendicular to the constituent layers, there is an exotic mode oscillating with each layer as a whole but alternatively from layer to layer. It belongs to the A_{1g} in the ENSGLs and A_2'' in the ONSGLs. Since the σ_h operation exists only in the ONSGLs, this mode (ω_1 mode) is Raman active in the ENSGLs while ir active in the ONSGLs.

In the *AA*-stacked NSGLs with N even or odd, the symmetry group is D_{6h} which includes both σ_i and σ_h. As a result, phonon modes cannot be ir and Raman active simultaneously. The ω_1 mode mentioned above belongs to the A_{1g} in the ENSGLs and A_{2u} in the ONSGLs. This mode is Raman active in the ENSGLs while ir active in the ONSGLs which is the same as the *AB*-stacked NSGLs. Nevertheless, its vibrational mode favors to take the maximum advantage of the interlayer interactions. It would be sensitive and useful experimentally to identify the even-oddness of the NSGLs with a few layers.

IV. CALCULATION FOR THE PHONON DISPERSION

A. Vibrational potential energy

The vibrational potential energy for a graphene sheet can be described by five quadratic terms with the rigid rotational symmetry implemented.[7,14] They are the first and second nearest-neighbor stretching, the in-plane bond angle variations, the out-of-surface bond bending, and the bond twisting energies. From the modality of atomic movements, we can also classify the interlayer vibrational potential terms into three types: The first one describes the stretching movements between the two atoms located in the adjacent layers. The second describes the relative movement between the two pairs of atoms with a common one as an apex; that is, this type of movement involves three atoms forming one bond in a layer and another connecting the two nearest layers. The third involves more than three atoms according to the specific bond configurations. As shown in Fig. 1, there is only one interlayer nearest-neighbor carbon-carbon bond in each unit cell (the bond between atoms 1 and 4), so that just the twisting potential on the interlayer bond is encountered here. The whole of these terms is actually a modified valence force field model to account some interactions for far away atoms in response to the bond charge effect a certain extent. Since the interlayer bonds are much longer than that in the plane, all above three type interactions are one or two orders less than their counterparts in layer and they themselves have comparable contributions. In the following, the interlayer terms are written in the *AB*-stacked system and they can be similarly generalized to the *AA*-stacked system.

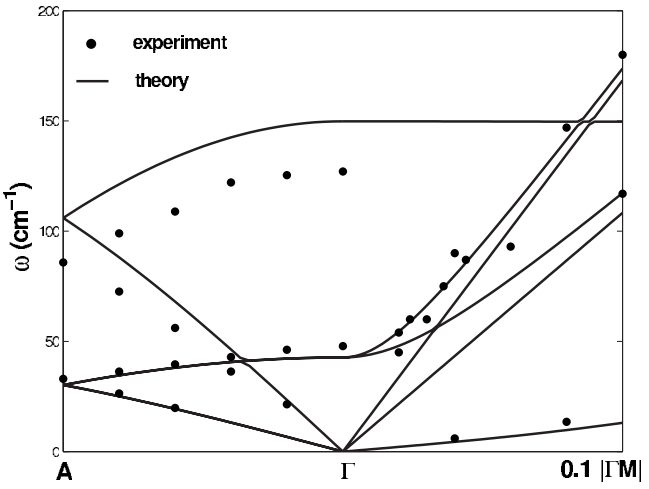

FIG. 2. Phonon dispersion for the 3D graphite in the low-frequency region. Solid dots are the experimental results of Ref. 19. Our theoretical calculations are shown as lines.

(i) The interlayer bond stretching energies $V_l^{(\mathrm{int})}/(V_{sl}^{(\mathrm{int})})$ have the form

$$\sum_{i,j} \frac{\hat{k}_l}{2}[(\vec{u}_i - \vec{u}_j)\cdot \vec{e}_{ij}^{\,l}]^2, \tag{1}$$

where $\vec{u}_i$ ($\vec{u}_j$) is the displacement vector of the atom i (j) and $\vec{e}_{ij}^{\,l}$ is the unit vector from atom i to atom j. If the summation is taken over the nearest-neighbor interlayer pair of atoms, the corresponding force constant is denoted as $\hat{k}_l$ while for next nearest-neighbor interlayer pairs we have the force constant $\hat{k}_{sl}$.

(ii) For the three atoms 1, 4, and i, where i is the in-plane nearest neighbor of atom 1 (see Fig. 1), we found that under a specific configuration with atom i rather than atom 1 as an

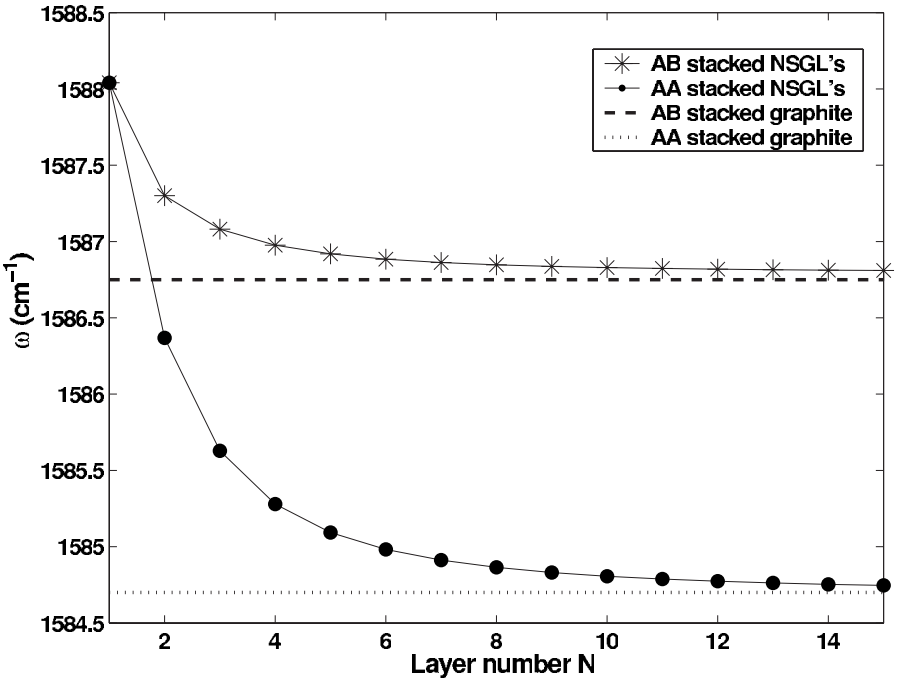

FIG. 3. Phonon dispersion for the 3D graphite in the high-frequency region. Solid dots are the experimental results (Refs. 20 and 21). In Refs. 20 and 21, those phonon wave vectors $\vec{q}$, which were not exactly along the Γ-M or Γ-K-M direction, were projected onto the closest high-symmetry direction. Lines are our theoretical calculations.

apex, whith the force being along the corresponding bond direction instead of the perpendicular direction, a correlation term $\hat{k}_{rr}$ has the most sensitive contribution to the layer dependence of the intralayer *C*-*C* stretching optical modes,

$$\frac{\hat{k}_{rr}}{2}\sum_i [(\vec{u}_1 - \vec{u}_i)\cdot \vec{e}^{\,l}_{i1} - (\vec{u}_4 - \vec{u}_i)\cdot \vec{e}^{\,l}_{i4}]^2.$$

Actually the two square terms in the above modality have already been accounted for in the in-plane and interplane stretching terms, respectively. Only the across term is left,

$$V_{rr} = -\hat{k}_{rr}\sum_i [(\vec{u}_1 - \vec{u}_i)\cdot \vec{e}^{\,l}_{i1}][(\vec{u}_4 - \vec{u}_i)\cdot \vec{e}^{\,l}_{i4}], \qquad (2)$$

which weakens the interaction between two adjacent layers. The positive-definite condition for getting real frequencies is $\hat{k}_{sl} \geq \hat{k}_{rr}$.

(iii) The twisting potential for an interlayer bond between atoms 1 and 4 is coming from the two sets of three nearest neighbors of atoms 1 and 4, respectively. It can be described as

$$V_{tw} = \frac{\hat{k}_{tw}}{2}\left[\sum_i (\vec{u}_i - \vec{u}_1)\cdot \vec{e}^{\,\theta}_i - \sum_j (\vec{u}_j - \vec{u}_4)\cdot \vec{e}^{\,\theta}_j\right]^2, \qquad (3)$$

where Σ_i and Σ_j represent the summation over the three intraplane first-nearest neighbors for atoms 1 and 4, respectively. $\vec{e}^{\,\theta}_i = \vec{e}_z \times \vec{e}^{\,l}_{1i}$ is the tangential unit vector in the plane formed by three atoms 1, 4, and *i*. The expression in quadratic form as a whole ensures a proper definition for the torsion angle. For pure rotations around the bond, this expression gives zero torsion consistently. In contrast, the bond is most severely twisted when the three neighbors around atom 1 and those of atom 4 rotate reversely.

We stress here that all of the above four interlayer vibrational potential-energy terms satisfy the rigid rotational symmetry requirements[14–16] which guarantees the existence of the flexure modes in the low dimensional systems. Although we establish the vibrational potential terms based on the analysis to the modality of movements, the bond charge effect especially along the perpendicular direction has been involved by extending the valence force field beyond the nearest neighbors. Comparing, for example, the above $\hat{k}_{rr}$ term with that of V_{b-b} in Ref. 17, which is followed from the bond-charge model, they have the same negative cross term.

B. Results and discussion

The five intralayer force constants we used in the following are taken from Ref. 18 with a minor modification. We

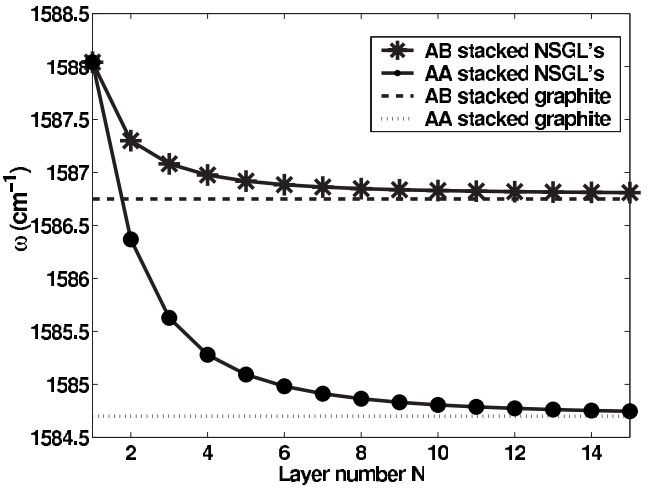

FIG. 4. The frequency value for the optical *C*-*C* stretching mode vs the layer number *N*. Lines are draw to guide the eyes.

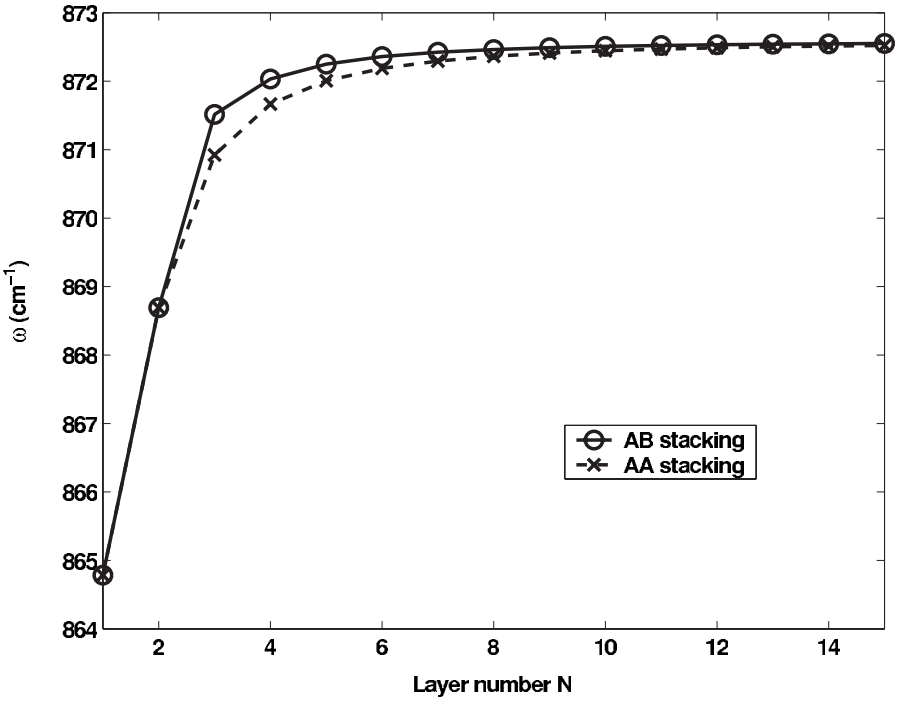

FIG. 5. The frequency value for the out-of-plane optical mode vs the layer number N. This mode is ir active in the AB stacking while it is neither ir nor Raman active in the AA stacking. Lines are drawn to guide the eyes.

adjust the four interlayer force constants to fit the experimental values of four modes in 3D graphite as shown in Table II. The fitting error for phonon modes is kept less than 7%. The interlayer force constants are then fitted as $\hat{k}_l$=0.77 N m^{-1}, $\hat{k}_{sl}$=0.95 N m^{-1}, $\hat{k}_{tw}$=0.64 N m^{-1}, and $\hat{k}_{rr}$=0.9 N m^{-1}.

Based on the above fitted vibrational potential energy with nine terms, we calculate the dispersion curves for the AB-stacked graphite. As illustrated in Figs. 2 and 3, our theoretical calculations meet the experimental results not only in the low-frequency[19] but also in the high-frequency regions.[20,21] The excellent consistency with the experimental data shows that our model and parameters are reasonable and applicable.

With the above force constants, we can calculate the phonon dispersion for NSGLs of the AA or AB stacking with an arbitrary layer number N. In Fig. 4, the calculated frequency of the intralayer optical C-C stretching mode is represented with different stacked styles and layer number N. The layer dependence of the frequency shows up as a redshift behavior which is in agreement with the experimental measurements. The frequency value for this mode is about 1588 cm^{-1} in the single graphene layer and decreases with increasing N and almost saturates at N=10. The limit is 1586.7 cm^{-1} (1584.7 cm^{-1}) in the AB- (AA-) stacked system, respectively. The amount of redshift value in our calculation corresponds excellently with that measured by experiments within the ranges 3–5, 5–6, and 8 cm^{-1} in Refs. 4–6, respectively.

The out-of-plane optical mode, belonging to the A_{2u} (B_{2g}) irreducible representation in the AB (AA) stacking, is ir active in the AB stacking yet inactive in the AA stacking irrespective of the even-oddness of the layer number N and is

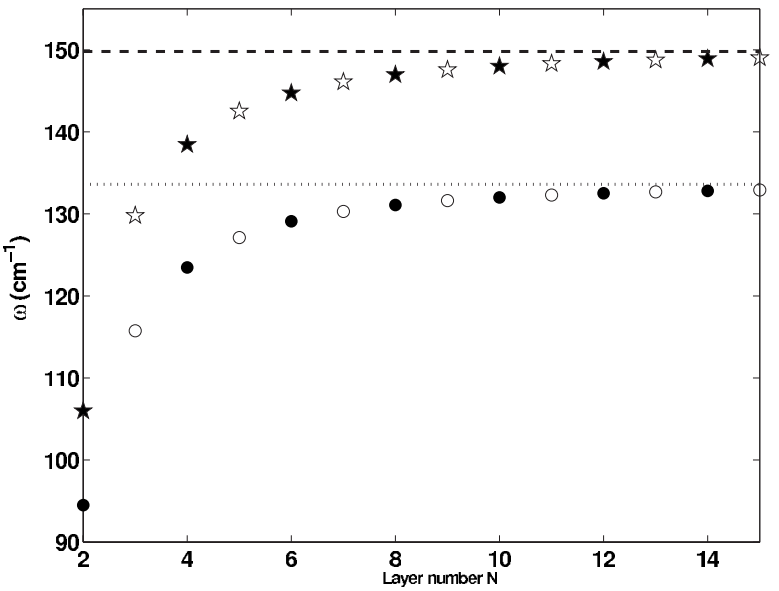

FIG. 6. The frequencies of the interlayer optical mode vs the layer number N. Data for the AB- and AA-stacked NSGLs are designated by pentagrams and circles, respectively. The Raman and infrared activities for this mode are displayed by the full and empty symbols, respectively. The broken and dashed lines correspond to the frequencies for the AB-stacked and AA-stacked graphite, respectively.

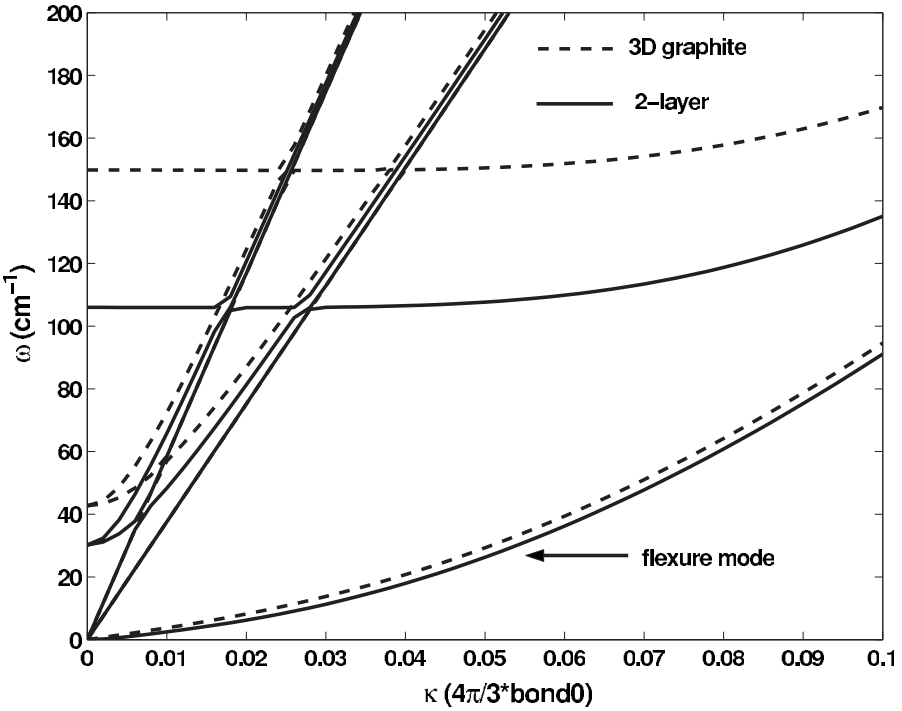

FIG. 7. In the low-frequency region, there is significant difference between 3D graphite and the two-layer graphene.

useful in determining whether the NSGLs are of *AB* or *AA* stacking. As shown in Fig. 5, frequencies for this mode depend on the layer number N and increase from 864.8 to 872.6 cm^{-1} in both the *AB* and *AA* stacking. In contrast to the *C*-*C* stretching optical mode, this mode frequency exhibits a blueshift type layer dependence which could be identified with the development of the experimental technique.

For the interlayer optical mode, the layer-number dependence of the frequency value is shown in Fig. 6. This mode takes the greatest advantage of the interlayer interaction and is considerably dependent on the layer number N and the stack style *AB* or *AA*. In case of $N=2$, the ω_1 mode has the frequency values 106 and 94.5 cm^{-1} for the *AB*- and *AA*-stacked NSGLs, respectively. The frequencies of the ω_1 mode increase with increasing N and almost come to the limit values at $N=10$. The limit values are 149.8 and 133.6 cm^{-1} for the *AB*- and *AA*-stacked NSGLs, respectively. The frequency differences as well as the Raman versus ir (see Sec. III) of the ω_1 mode in NSGLs with different layers might inspire considerably experimental interest in the ω_1 mode.

We then calculate the phonon dispersion for the two-layered *AB* stacking, in comparison with that of the 3D graphite. The most significant difference between the two-layer graphene and the 3D graphite lies in the low-frequency region around the Γ point as shown in Fig. 7. The frequencies of the low-frequency optical modes in the two-layer graphene are much smaller than their counterparts in the 3D

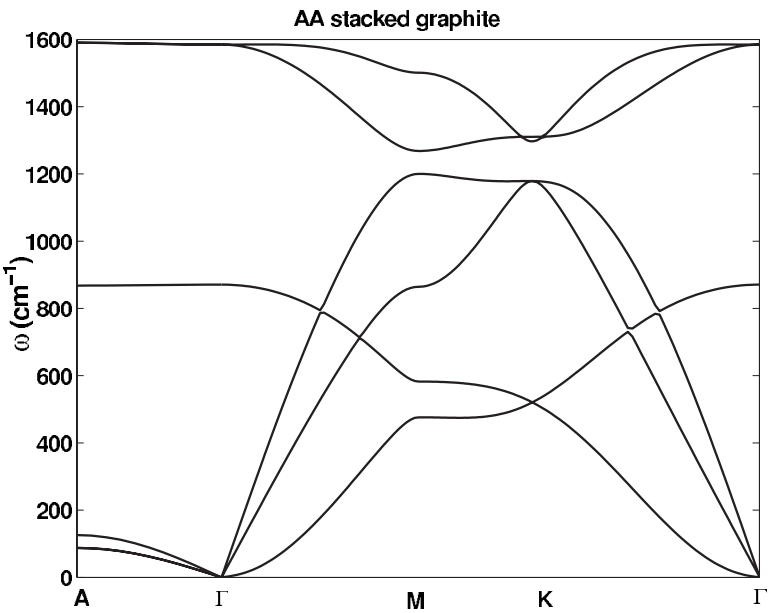

FIG. 8. The phonon dispersion along some high-symmetry directions for the *AA*-stacked 3D graphite. There are only six branches in the figure, since the unit cell in the *AA*-stacked 3D graphite contains two atoms.

TABLE III. The Raman and ir mode frequencies (in the unit of cm^{-1}) for the *AB*-stacked 3D graphite, *AB*-stacked two-layer graphene, and *AA*-stacked 3D graphite are listed. The irreducible representations are presented in the brackets following the frequency values.

	Raman		Infrared	
AB-3D	42.7 (E_{2g})	1586.7 (E_{2g})	869.9 (A_{2u})	1588.2 (E_{1u})
AB	30.2 (E_g)	106 (A_{1g})	868.7 (A_{2u})	1588.1 (E_u)
Two-layer	867.4 (A_{1g})	1587.3 (E_g)		
AA-3D	1584.7 (E_{2g})			

graphite. The frequencies of the Raman and ir active modes are shown in the third line of Table III among which the two A_{1g} modes have the frequency value $\omega_1=106\ cm^{-1}$ and $\omega_2=867.4\ cm^{-1}$. In fact, ω_1 and ω_2 modes are the above mentioned NA_{1g} modes of the ENSGLs specified to $N=2$.

We further calculate the phonon-dispersion curve for the *AA*-stacked 3D graphite as shown in Fig. 8. Since the unit cell contains only two atoms in contrast to that of the *AB*-stacked graphite, there are six branches of phonon dispersion. Along ΓA in the Brillouin zone, the lowest and highest branches which correspond to the in-plane acoustic and optical vibrational modes are doubly degenerate, while the remaining two branches describing the out-of-plane vibration are nondegenerate. At the *A* point in the Brillouin zone, there is a phase factor difference of π between two adjacent layers for the out-of-plane motion, among which the ω_1 mode has the frequency value of $133.6\ cm^{-1}$. In the fourth line of Table III, the Raman and ir active modes for the *AA*-stacked 3D graphite are listed, which are to be confirmed in future experiments.

V. CONCLUSION

Based upon a thorough investigation of the lattice symmetry of the NSGLs, the Raman and ir properties, in particular, layer dependence, are systematically studied. With a proposed generalized vibrational potential, we further calculate the phonon dispersion of various modes of the *AB*- or *AA*-stacked NSGLs where the layer dependence is also stressed. The calculated frequencies of the optical *C*-*C* stretching mode exhibit a redshift as the layer number increases in both the *AB*- and *AA*-stacked NSGLs, and the shift value 2 cm^{-1} (4 cm^{-1}) for *AB*- (*AA*-) stacked NSGLs is in good consistency with the experimental measurements. The out-of-plane optical mode with frequency around about 800 cm^{-1} is ir active in the *AB*-stacked structure yet neither Raman nor ir active in *AA* stacking. Its frequency shows a blueshift layer dependence. We also predict that the frequency of the interlayer optical mode increases with increasing *N*. Since this mode is more sensitive to the layer number *N*, it should be experimentally interesting in determining the lattice structure properties of the NSGLs.

As a kind of force-constant model, our generalized vibrational potential model, which is successful in the study of the vibrational properties of the NSGLs shown above, is based on the analysis to the different atomic modalities in small vibrations and the ensuring of various symmetry requirements of lattice configuration. Generally, each type of atomic modalities is described by a quadratic form of the lattice displacement that often includes the nearest-neighbor or next-nearest-neighbor atom pairs. Such *ad hoc* models are actually phenomenological with their parameters fitted by the experimental data. They have the advantage of being physically intuitive in describing and understanding the vibrational properties, while the identification of modalities with their correspondence quadratic forms is empirical and it is not easy to set out a theoretical criterion to guarantee the completeness and correctness of extracted forms. Therefore, to study accurately the various aspects of vibrational properties of carbon networks, sophisticated and systematic treatments with many couplings are extremely beneficial.

*jwjiang@itp.ac.cn

[1] K. S. Novoselov, A. K. Geim, S. V. Morozov, D. Jiang, Y. Zhang, S. V. Dubonos, I. V. Grigorieva, and A. A. Firsov, Science **306**, 666 (2004).
[2] C. Berger, Z. Song, T. Li, X. B. Li, Asmerom Y. Ogbazghi, R. Feng, Z. T. Dai, Alexei N. Marchenkov, Edward H. Conrad, Phillip N. First, and Walt A. de Heer, J. Phys. Chem. B **108**, 19912 (2004).
[3] B. Partoens and F. M. Peeters, Phys. Rev. B **74**, 075404 (2006); **75**, 193402 (2007).
[4] A. C. Ferrari, J. C. Meyer, V. Scardaci, C. Casiraghi, M. Lazzeri, F. Mauri, S. Piscanec, D. Jiang, K. S. Novoselov, S. Roth, and A. K. Geim, Phys. Rev. Lett. **97**, 187401 (2006).
[5] A. Gupta, Gugang Chen, P. Joshi, S. Tadigadapa, and P. C. Eklund, Nano Lett. **6**, 2667 (2006).
[6] Anindya Das, Biswanath Chakraborty, and A K. Sood (unpublished).
[7] T. Aizawa, R. Souda, S. Otani, Y. Ishizawa, and C. Oshima, Phys. Rev. B **42**, 11469 (1990); **43**, 12060(E) (1991).
[8] R. Saito, G. Dresselhaus, and M. S. Dresselhaus, *Physical Properties of Carbon Nanotubes* (Imperial College, London, 1998).
[9] L. Brillson, E. Burskin, A. A. Maradudin, and T. Stark, in *The Physics of Semimetals and Narrow-Gap Semiconductors*, edited by D. L. Carter and R. T. Bate (Pergamon, London, 1971).
[10] J. L. Manes, F. Guinea, and Maria A. H. Vozmediano, Phys. Rev. B **75**, 155424 (2007).
[11] J. P. Elliott and P. G. Dawber, *Symmetry in Physics* (Macmillan, London, 1979), Vol. 1.
[12] H. Eyring, J. Walter, and G. Kimball, *Quantum Chemistry* (Wiley, New York, 1940).
[13] K. K. Mani and R. Ramani, Phys. Status Solidi B **61**, 659 (1974).
[14] J. W. Jiang, H. Tang, B. S. Wang, and Z. B. Su, Phys. Rev. B **73**, 235434 (2006).

[15] V. N. Popov, V. E. Van Doren, and M. Balkanski, Phys. Rev. B **61**, 3078 (2000).
[16] G. D. Mahan and Gun Sang Jeon, Phys. Rev. B **70**, 075405 (2004).
[17] Gun Sang Jeon and G. D. Mahan, Phys. Rev. B **72**, 155415 (2005).
[18] Jin-Wu Jiang, Hui Tang, Bing-Shen Wang, and Zhao-Bin Su, J. Phys.: Condens. Matter **20**, 045228 (2008).
[19] R. Nicklow, N. Wakabayashi, and H. G. Smith, Phys. Rev. B **5**, 4951 (1972).
[20] J. Maultzsch, S. Reich, C. Thomsen, H. Requardt, and P. Ordejon, Phys. Rev. Lett. **92**, 075501 (2004).
[21] M. Mohr, J. Maultzsch, E. Dobardzic, S. Reich, I. Milosevic, M. Damnjanovic, A. Bosak, M. Krisch, and C. Thomsen, Phys. Rev. B **76**, 035439 (2007).